Electronic Supplementary Material (ESI) for Journal of Materials Chemistry A.

Supporting Information

Metallic 1T-MoS_2 coupled on MXene towards ultra-high rate-capability for supercapacitor

Feng Wan,[a] Xin Wang,*[a] Can Tang,[a] Chengzhong Jiang,[a] Weixin Wang,[a] Bing Li,[a] Yongxing Zhang,*[a] and Xuebin Zhu[b]

[a]Anhui Province Key Laboratory of Pollutant Sensitive Materials and Environmental Remediation, Department of Materials Science & Engineering, School of Physics and Electronic Information, Huaibei Normal University, Huaibei 235000, P. R. China.

[b] Key Laboratory of Materials Physics, Institute of Solid State Physics, Hefei Institute of Physical Science, Chinese Academy of Sciences, Hefei 230031, People's Republic of China

***Corresponding author E-mail:** wkangxin@163.com; zyx07157@mail.ustc.edu.cn.

Experimental Methods：

Material preparation

Preparation of 2H-MoS_2 Nanosheets. $(NH_4)_6Mo_7O_{24}\cdot 4H_2O$ (CAS number:12054-85-2) and thiourea (CAS number:6256-6) are purchased from Sinopharm. All chemicals are used without further treatment. 1.4484 g $(NH_4)_6Mo_7O_{24}\cdot 4H_2O$ and 2.8418 g thiourea were dissolved in deionized water (43.6 mL) and stirred vigorously for 30 min to get a homogeneous solution. After the mixture was transferred to a Teflon-lined stainless-steel autoclave (100 mL). Then, it was heated to 210℃ in 40 min and kept for 18 h. The resulting product was filtered, washed several times by deionized water and ethanol, and dried at 60℃ in a vacuum oven. Finally, the dried sample was ground into powder in an agate mortar with an inner diameter of 90mm to obtain 2H-MoS_2 nanosheets.

Preparation of 1T-MoS_2 Nanosheets. Urea (CAS number:57-13-6), MoO_3 (99.5%) and thioacetamide (≥99.0%) are purchased from Sinopharm, Colloid chemical plant of Shanghai Huayi Group Huayuan Chemical Co., Ltd., and Tianjin Guangfu Fine Chemical Research Institute, respectively. All chemicals are used without further treatment. 1.2 g Urea, 0.79 g MoO_3 and 0.42 g Thioacetamide were dissolved in deionized water (60 mL) and stirred vigorously for 30 min to get a homogeneous solution. After the mixture was transferred to a Teflon-lined stainless-steel autoclave (100 mL). Then, it was heated to 200℃ in 40 min and kept for 12 h. The resulting product was filtered, washed several times by deionized water and ethanol, and dried at 60℃ in a vacuum oven. Finally, the dried sample was ground into powder in an agate mortar with an inner diameter of 90mm to obtain 1T-MoS_2 nanosheets.

Preparation of 1T-MoS_2/$Ti_3C_2T_x$ composite material. $Ti_3C_2T_x$ was purchased by Shandong xiyan new material technology co. LTD. Urea, MoO_3 and thioacetamide were dissolved in 60 mL deionized water (the usage is consistent with the synthesis of 1T-MoS_2), 0.06 g $Ti_3C_2T_x$ were further added to the solution stirred vigorously for 30 min to get a homogeneous solution. After that, the following experimental procedure is consistent with the synthesis of 1T-MoS_2. The mass of as-synthesized 1T-MoS_2/$Ti_3C_2T_x$ powder is about 0.34g. Therefore, the weight percentages of Ti_3C_2 MXene and 1T-MoS_2 in the 1T-MoS_2/$Ti_3C_2T_x$ composite are respectively about 17.6% ($\frac{0.06\ g}{0.34\ g}\times 100\%$) and 82.4% ($\frac{0.34\ g-0.06\ g}{0.34\ g}\times 100\%$), and the mass ratio Ti_3C_2 MXene to 1T-MoS_2 is about 17.6%: 82.4%. Furthermore, the mass

ratio of element Ti to Mo in 1T-MoS_2/$Ti_3C_2T_x$ sample are according to the following equations:

$$\frac{m_{Ti}}{m_{Mo}} = \frac{m_{Ti_3C_2} \times \frac{M_{Ti} \times 3}{M_{Ti_3C_2}}}{m_{MoS_2} \times \frac{M_{Mo} \times 1}{M_{MoS_2}}} \quad (1)$$

Where M_{Mo}, M_{Ti}, M_{MoS_2} and $M_{Ti_3C_2}$are molar mass of Mo (95.9), Ti (47.9), MoS_2 (160.1) and Ti_3C_2 (167.7), $m_{Ti_3C_2}$ and m_{MoS_2} are the mass of $Ti_3C_2T_x$ (0.06 g) and 1T-MoS_2 ($0.34\ g - 0.06\ g = 0.28\ g$), respectively. Therefore, the mass ratio of element Ti to Mo in 1T-MoS_2/$Ti_3C_2T_x$ sample is about 30:100. Additionally, the content of Ti and Mo element in 1T-MoS_2/$Ti_3C_2T_x$ sample had been characterized by inductively coupled plasma-optical emission spectroscopy (ICP-OES). The test data are shown in the table and the mass ratio of element Ti to Mo is about 26:100 ($\frac{106726.09\ mg/Kg}{406077.80\ mg/Kg}$), which is approximately consistent with the above results (30:100).

Preparation of δ-MnO_2 material. Potassium permanganate (CAS number:7722-64-7, 99.5%) and CTAB (CAS number:57-09-0, 99.0%) are purchased from Sinopharm. All chemicals are used without further treatment. 0.63 g Potassium permanganate and 0.04 g CTAB were dissolved in deionized water (30 mL) and stirred vigorously for 30 min to get a homogeneous solution. After the mixture was transferred to a Teflon-lined stainless-steel autoclave (50 mL capacity). Then, it was heated to 140℃ in 30 min and kept for 12 h. The resulting product was filtered, washed several times by deionized water and ethanol, and dried at 60℃ in a vacuum oven. Finally, the dried sample was ground into powder in an agate mortar with an inner diameter of 90mm to obtain δ-MnO_2 nanosheets.

Materials Characterizations

Phase, crystal structure, and microscopic morphology characterizations of samples were conducted by X-ray diffraction (XRD, PANalytical Empyrean) patterns with Cu K radiation, λ = 0.15406 nm, Field emission scanning electron microscope (FESEM, HiTACHI Regulus8220) and Energy-

dispersive X-ray spectroscopy (EDX, Oxford EDX, with INCA software), transmission electron microscope (TEM, JEOL JEM-2100) with configured EDX, X-ray photoelectron spectroscopy (XPS, AXIS SUPRA+ equipped with monochromatic Al Kα source). Raman spectroscopy was carried out by a LabRAMHR800 UV NIR spectrometer with 532 nm laser excitation. As for the conductivity measurements, Firstly, the corresponding powders were coldly pressed into compact sheets using a holder. After that, the wafers were cut into rectangular strips. Secondly, four gold wires were attached to the rectangular strips with silver glue. And then, the strips are mounted onto the holder of the physical property measurement system (PPMS). Thirdly, the room-temperature resistance (R) was measured by using PPMS. After that, we measured the length (L) and cross-sectional area (S) of the rectangular strip. And then, the resistivity can be obtained by $\rho = R\frac{S}{L}$. Finally, the conductivity (σ) can be calculated by $\sigma = \frac{1}{\rho}$. The part of electrochemical measurement was performed by the electrochemical workstation CHI-760E.

Electrochemical tests

For the electrochemical tests of 2H-MoS_2, 1T-MoS_2, $Ti_3C_2T_x$, 1T-MoS_2/Ti_3C_2 MXene and δ-MnO_2 electrodes, the working electrodes in a three-electrode configuration were fabricated as followings: a mixture of active material (2H-MoS_2, 1T-MoS_2, $Ti_3C_2T_x$, 1T-MoS_2/Ti_3C_2 MXene or δ-MnO_2), polyvinylidene fluoride (PVDF) and carbon black with a weight ratio of 8: 1: 1 was uniformly cast on carbon papers. The conductivity of the carbon paper (Toray, Japan) can reach ~ 17 240 S m^{-1}. The area of the working electrodes is ~1 cm^2, and the mass of loading of electrodes is 1~1.5 mg. Then the electrodes were dried in vacuum oven at 60 °C for 24 hours. Platinum and Ag/AgCl in 1 M KCl were used as the counter electrode and reference electrode, respectively. The gravimetric specific capacitance calculated from from the galvanostatic charge-discharge (GCD) curves is given by:

$$C = jt/\Delta V \qquad (2)$$

and it can be calculated from the cyclic voltammetry (CV) curves is given by:

$$C = \frac{1}{\Delta V}\int \frac{jdV}{v} \qquad (3)$$

Here, C is the specific capacitance (F g^{-1}), ΔV is the potential window (V), v is the scan rate (V s^{-1}), V is the potential (V), j is the current density (A g^{-1}), and t is time (s). Electrochemical impedance

spectroscopy (EIS) was performed with open circuit voltage in frequency range of 100 kHz to 0.01 Hz. All tests were performed using the CHI 760E electrochemical work station in 1 M Na_2SO_4 electrolyte.

Preparation of PVA-Na_2SO_4 gel: Firstly, 1 g of polyvinyl alcohol (PVA) powder was dissolved into 10 mL of DI water, and the mixture was heated to 90°C under exquisite stirring until the solution became clear. Then, the Na_2SO_4 (1 M) was added dropwise into the above solution under constant stirring. To prepare the flexible electrodes, the slurry of the negative material 1T-MoS_2/$Ti_3C_2T_x$ and the positive material δ-MnO_2 is uniformly coated on the flexible carbon cloth, respectively. Then the carbon cloth coated with slurry is dried in a vacuum drying oven at 60°C for 24 hours. Subsequently, a 1T-MoS_2/$Ti_3C_2T_x$ flexible electrode and a δ-MnO_2 electrode which are coated with PVA-Na_2SO_4 gel were assembled into a supercapacitor by sandwiching cellulose membrane as separator between them. In order to achieve the best electrochemical performance of the 1T-MoS_2/$Ti_3C_2T_x$//δ-MnO_2 flexible asymmetric supercapacitor (FASC) device, the charge balance is determined as $q^+=q^-$. To achieve $q^+=q^-$, the mass of the active material on the electrode definitely is:

$$\frac{m_+}{m_-}=\frac{C_{electrode-}\times\Delta V_-}{C_{electrode+}\times\Delta V_+} \qquad (4)$$

Therefore, it was found that the positive and negative mass ratio of the 1T-MoS_2/$Ti_3C_2T_x$//δ-MnO_2 hybrid device is about 4: 5. After the PVA-Na_2SO_4 gel solidified at room temperature for ~12 h, the flexible asymmetric supercapacitor (FASC) was obtained.

The areal specific capacitance of the device based on area of the active material was calculated from charge-discharge curves according to the following equation:

$$C=\frac{I\times\Delta t}{S\times\Delta V} \qquad (5)$$

where I is the constant discharge current (A); Δt is the time for a full discharge (s); S is the facing area of the active material on the two working electrodes (cm^2); and ΔV is the voltage drop on discharge (V). The areal energy densities (E = μWh cm^{-2}) and power densities (P = μW cm^{-2}) of the ASC device were calculated using the following equations:

$$E=1/(2\times3.6)\times C\times\Delta V^2 \qquad (6)$$

$$P=3600\times E/\Delta t \qquad (7)$$

Here, *C* is the areal specific capacitance of the FASC device, ΔV is the potential window during the discharging process, *Δt* is the time for a full discharge of device. The CV, GCD and cyclic stability tests of FASC devices assembled with 1T-MoS_2/$Ti_3C_2T_x$ and δ-MnO_2 as electrodes were performed using the CHI 760E electrochemical work station.

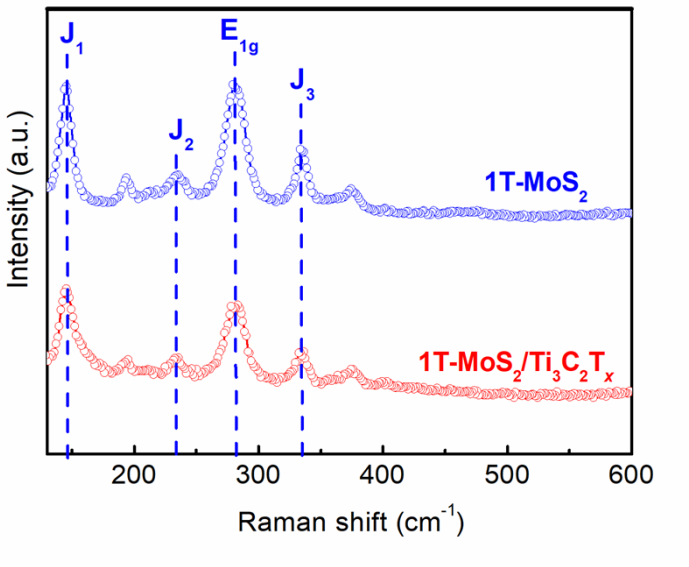

Figure S1. Raman spectrums of 1T-MoS_2 and 1T-MoS_2/$Ti_3C_2T_x$

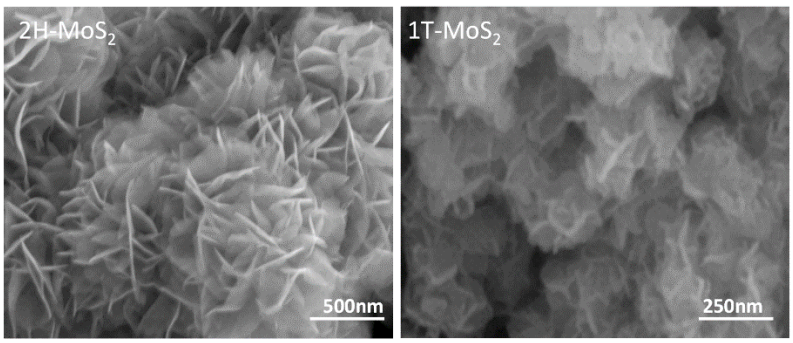

Figure S2. Scanning electron microscopy (SEM) images of 2H-MoS_2 and 1T-MoS_2

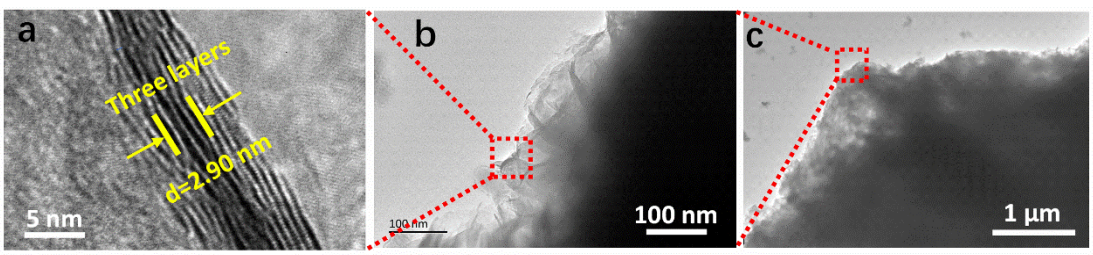

Figure S3. HRTEM image (a) and TEM images (b, c) of 1T-MoS_2/$Ti_3C_2T_x$ sample.

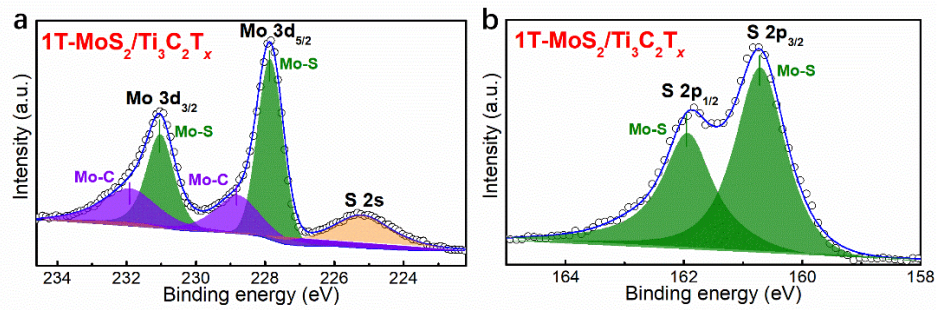

Figure S4. High-resolution Mo 3d and S2p spectra of the 1T-MoS_2/$Ti_3C_2T_x$

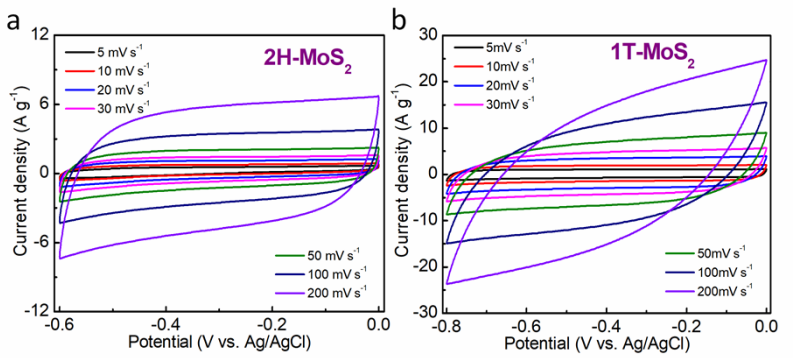

Figure S5. CV curves of 2H-MoS_2 and 1T-MoS_2 electrodes at 5-200 mV s^{-1}

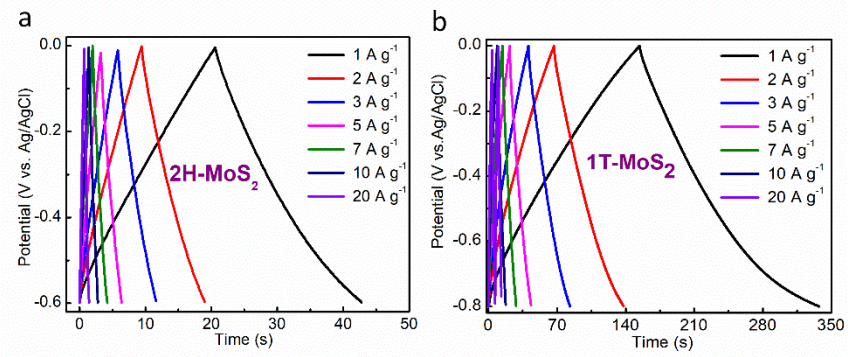

Figure S6. Galvanostatic charge-discharge (GCD) curves of $Ti_3C_2T_x$, 1T-MoS_2 and 1T-MoS_2/$Ti_3C_2T_x$ electrodes at different current densities of 1, 2, 3, 5, 7, 10 and 20 A g^{-1}

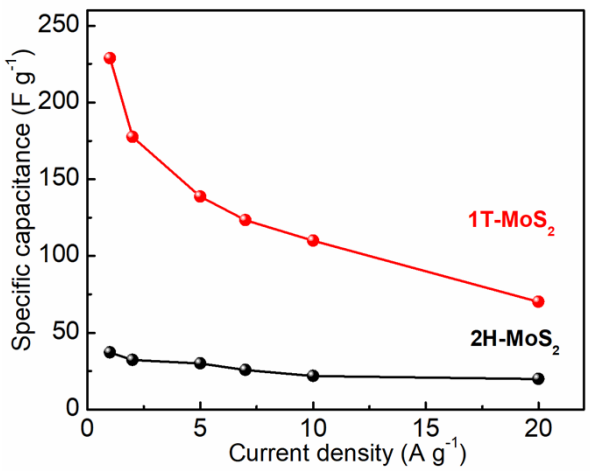

Figure S7. Rate capability of 2H-MoS_2 and 1T-MoS_2 electrodes from 2 A g^{-1} to 20 A g^{-1}.

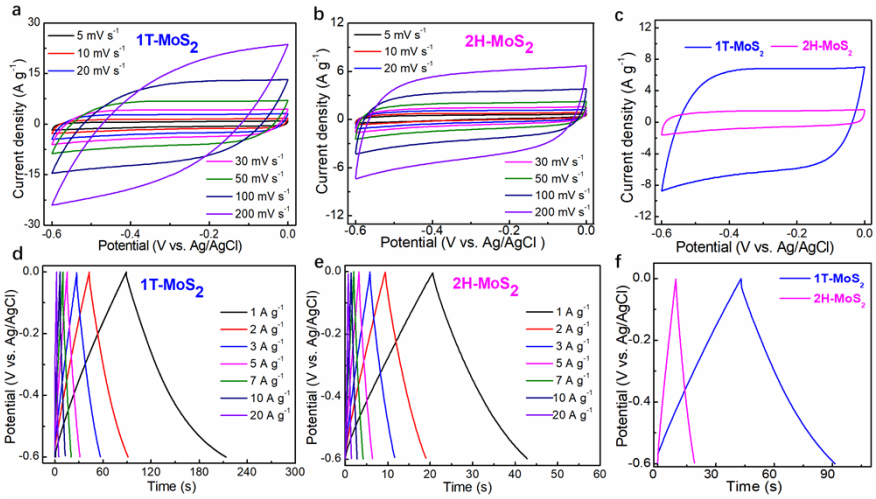

Figure S8 (a, b) CV and (d, e) GCD curves of 1T-MoS_2 and 2H-MoS_2, comparison of (c) CV curves at 50 mV s^{-1} and GCD curves at 2 A g^{-1} for 1T-MoS_2 and 2H-MoS_2.

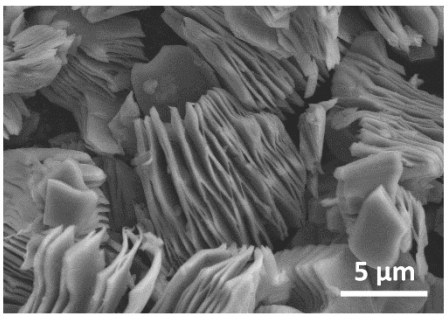

Figure S9. Scanning electron microscopy (SEM) images of $Ti_3C_2T_x$

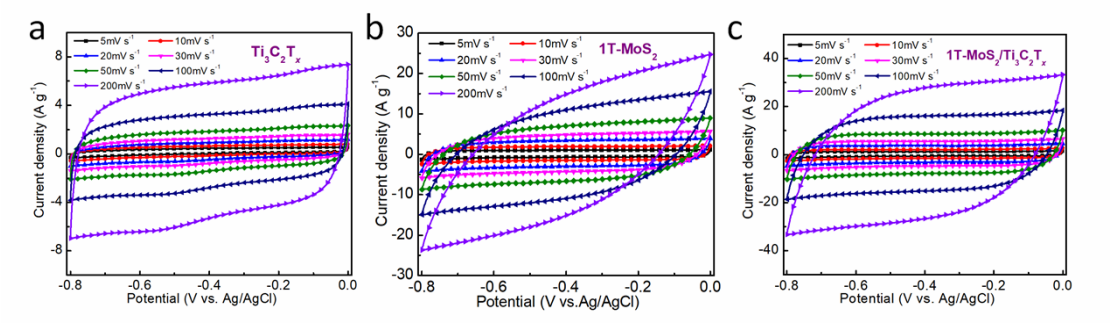

Figure S10. CV curves of $Ti_3C_2T_x$, 1T-MoS_2 and 1T-MoS_2/$Ti_3C_2T_x$ at 5-200 mV s^{-1}

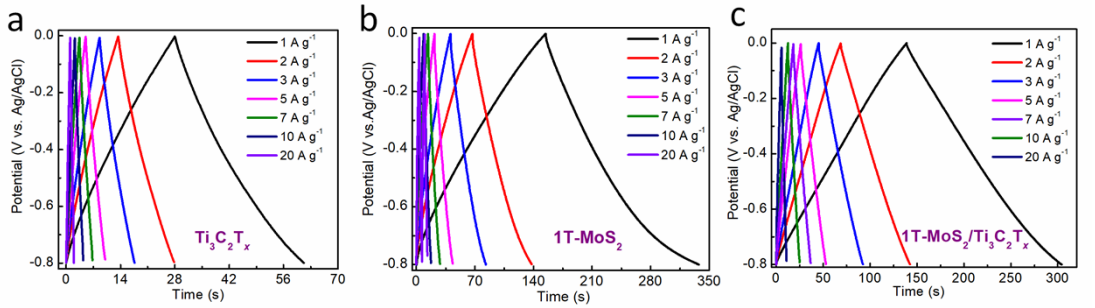

Figure S11. GCD curves of $Ti_3C_2T_x$, 1T-MoS_2 and 1T-MoS_2/$Ti_3C_2T_x$ at 1-20 A g^{-1}

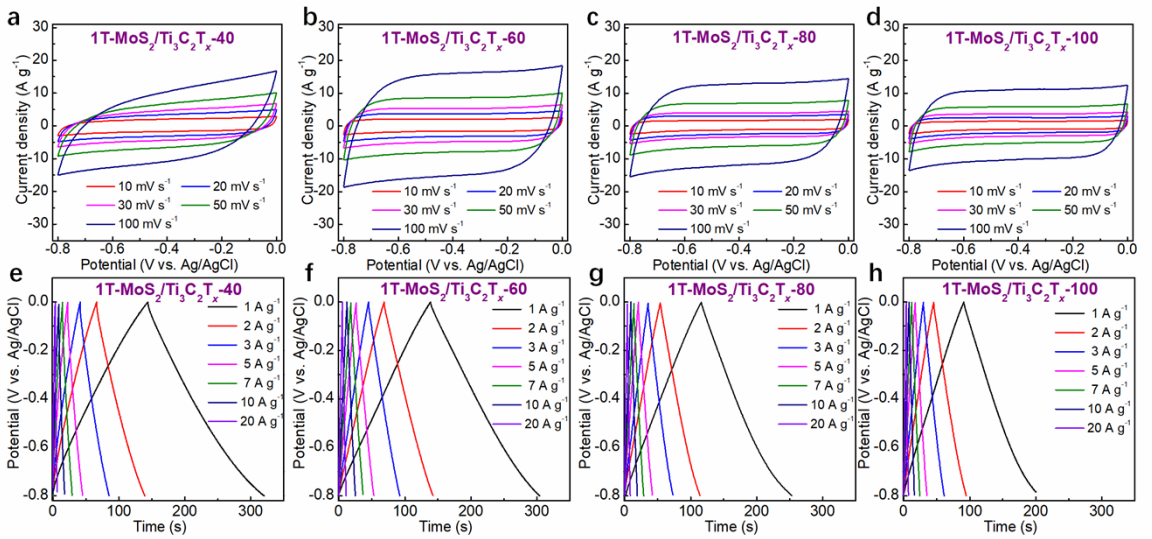

Figure S12. (a-d) CV and (e-h) GCD curves of 1T-MoS_2/$Ti_3C_2T_x$-40, 1T-MoS_2/$Ti_3C_2T_x$-60, 1T-MoS_2/$Ti_3C_2T_x$-80, 1T-MoS_2/$Ti_3C_2T_x$-100, respectively.

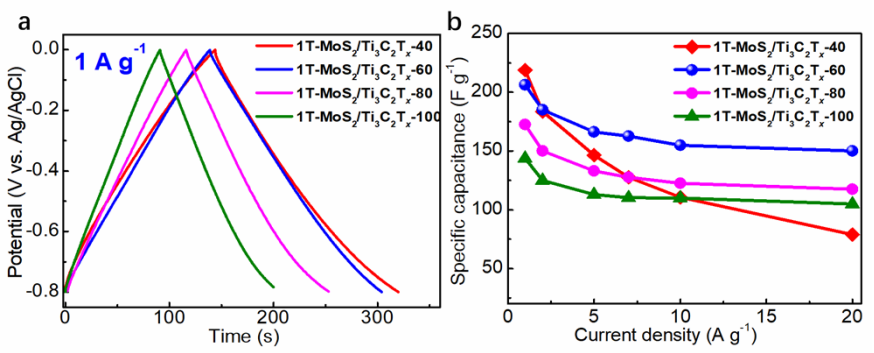

Figure S13. Comparison of (a) GCD curves at 1 A g^{-1} and (d) rate capability for 1T-$MoS_2/Ti_3C_2T_x$-40, 1T-$MoS_2/Ti_3C_2T_x$-60, 1T-$MoS_2/Ti_3C_2T_x$-80, 1T-$MoS_2/Ti_3C_2T_x$-100.

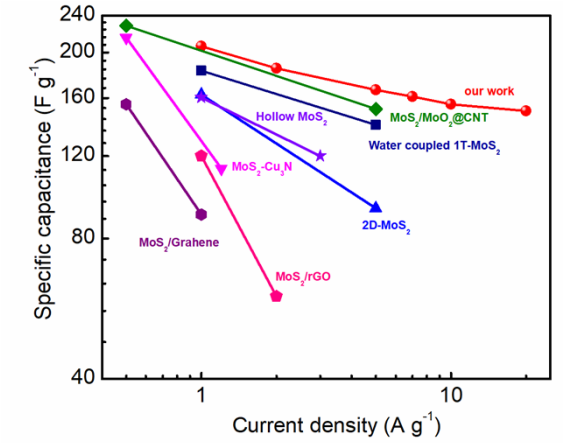

Figure S14. Ragone plots of Specific capacitance of 1T-$MoS_2/Ti_3C_2T_x$ compared to previously reported MoS_2-based electrode materials.

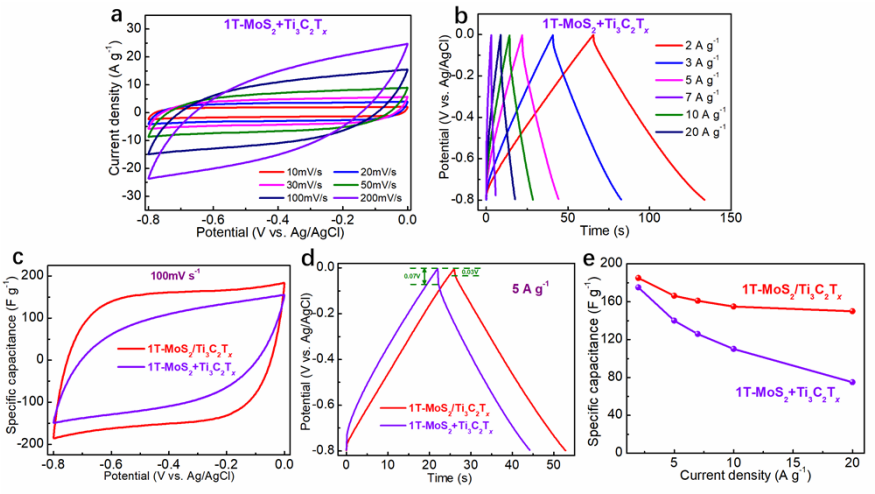

Figure S15. CV (a) and GCD (b) curves of the electrode prepared by mechanically mixing 1T-MoS_2 and $Ti_3C_2T_x$ (1T-MoS_2+$Ti_3C_2T_x$). Comparison of CV (c), GCD (d) curves and rate capability (e) for 1T-$MoS_2/Ti_3C_2T_x$ heterostructures and 1T-MoS_2+$Ti_3C_2T_x$ electrodes

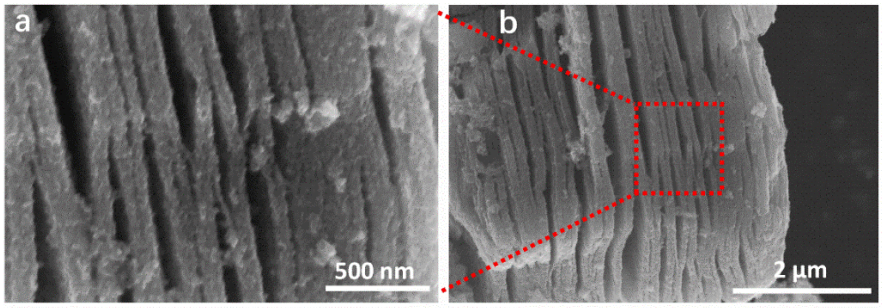

Figure S16. SEM images of 1T-MoS_2/$Ti_3C_2T_x$ heterostructure after long-cycling.

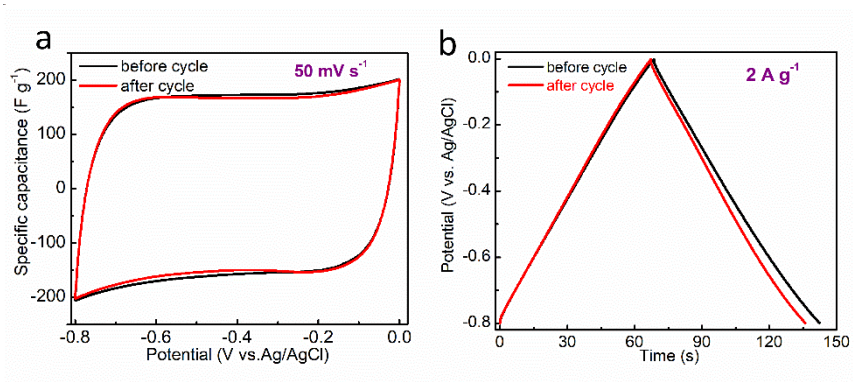

Figure S17. CV and GCD curves of 1T-MoS_2/$Ti_3C_2T_x$ electrode before and after cycling.

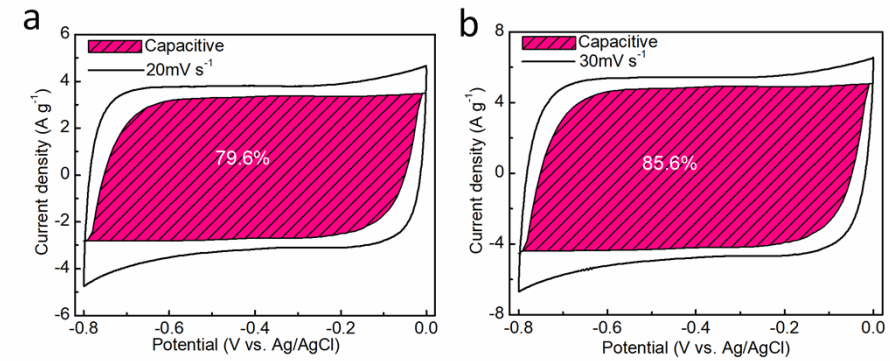

Figure S18. The capacitive contribution of 1T-MoS_2/$Ti_3C_2T_x$ electrode at 20 and 30 mV s^{-1}

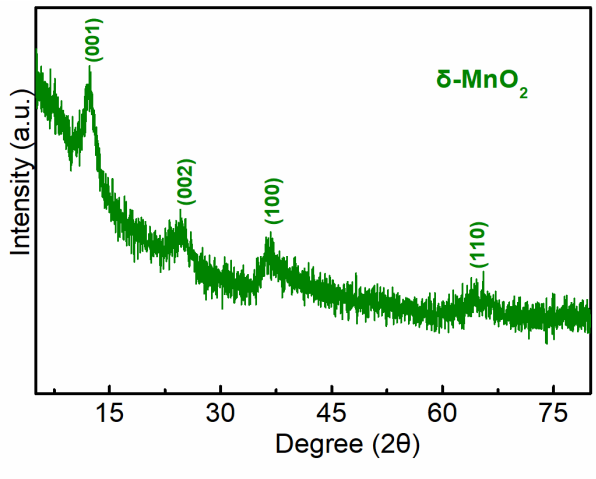

Figure S19. XRD results of δ-MnO_2

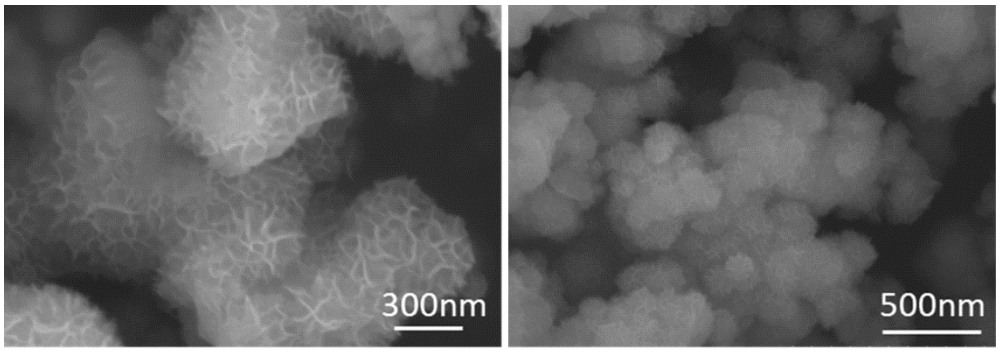

Figure S20. Scanning electron microscopy (SEM) images of δ-MnO_2

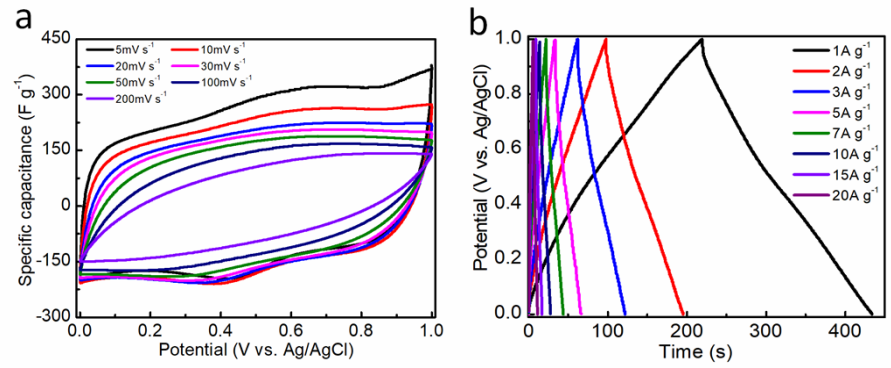

Figure S21. (a) CV curves of δ-MnO_2. (b) GCD curves of δ-MnO_2.

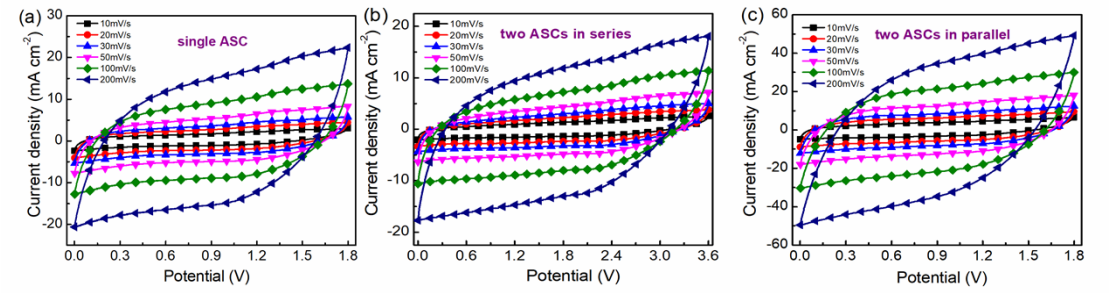

Figure S22. (a) CV curves of a single 1T-MoS_2/$Ti_3C_2T_x$//δ-MnO_2 FASC device. (b) CV curves of two devices in series. (c) CV curves of two devices in parallel.

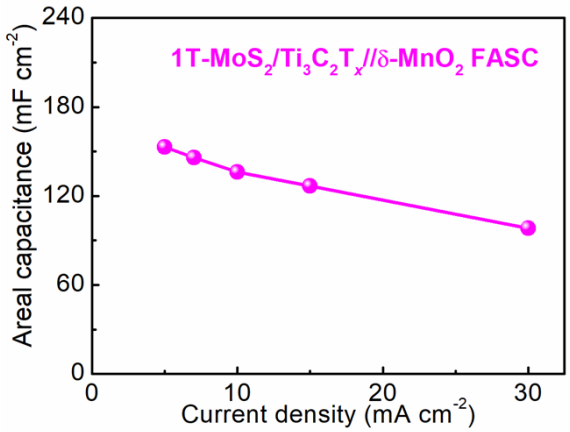

Figure S23. Areal specific capacitance of 1T-MoS_2/$Ti_3C_2T_x$//δ-MnO_2 FASC device at a series of current densities.

Table S1 The ICP-OES data of 1T-MoS_2/$Ti_3C_2T_x$ sample.

Mass of sample	Constant volume	Element	Element concentration	Dilution multiple	Element content
0.0617 g	25 mL	Ti	2.634 mg/L	100	106726.09 mg/kg
0.0617 g	25 mL	Mo	10.022 mg/L	100	406077.80 mg/kg

Table S2. Specific capacitances of $Ti_3C_2T_x$, 2H-MoS_2, 1T-MoS_2 and 1T-MoS_2/$Ti_3C_2T_x$ electrodes.

	1 A g^{-1}	2 A g^{-1}	5 A g^{-1}	7 A g^{-1}	10 A g^{-1}	20 A g^{-1}
$Ti_3C_2T_x$	43.1 F g^{-1}	38.3 F g^{-1}	33.7 F g^{-1}	32.4 F g^{-1}	30.9 F g^{-1}	28.4 F g^{-1}
2H-MoS_2	37.3 F g^{-1}	32.3 F g^{-1}	30 F g^{-1}	25.7 F g^{-1}	21.7 F g^{-1}	20 F g^{-1}
1T-MoS_2	228.8 F g^{-1}	177.5 F g^{-1}	138.8 F g^{-1}	123.4 F g^{-1}	110 F g^{-1}	70 F g^{-1}
1T-MoS_2/$Ti_3C_2T_x$	206.3 F g^{-1}	185 F g^{-1}	166.3 F g^{-1}	161 F g^{-1}	155 F g^{-1}	150 F g^{-1}

Table S3. Comparisons about specific capacitance of 1T-MoS_2/$Ti_3C_2T_x$ electrode with those of MoS_2-based electrode materials reported recently.

Electrode materials	Specific capacitance	Refs.
1T-MoS2@$Ti_3C_2T_x$	206.3 F g^{-1} at 1 A g^{-1} 166.3 F g^{-1} at 5 A g^{-1}	Our work
MoS_2/rGO	120 F g^{-1} at 1 A g^{-1} 60 F g^{-1} at 1 A g^{-1}	*J. colloid interf. sci.* **2018**, 518, 234.
2D-MoS_2	162.4 F g^{-1} at 1 A g^{-1} 92.7 F g^{-1} at 5 A g^{-1}	*Mater. Today: Proceedings 2020, **26**, 20.*
MoS_2–Cu_3N	215.47 F g^{-1} at 0.5 A g^{-1} 112.84 F g^{-1} at 1.2 A g^{-1}	*Appl. Phys. Lett.* **2021**,118, 203901.
MoS_2/MoO_2@CNT	228.4 F g^{-1} at 0.5 A g^{-1} 151.5 F g^{-1} at 5 A g^{-1}	*J. Mater. Chem. C* **2019**, **7**, 9545.
Water coupled 1T-MoS_2	183 F g^{-1} at 1 A g^{-1} 140 F g^{-1} at 5 A g^{-1}	*Nano Lett.* **2017**, 17, 1825
Hollow MoS_2	160.1 F g^{-1} at 1 A g^{-1} 120 F g^{-1} at 3 A g^{-1}	*Mater. Lett.* **2016**, 184, 96.
MoS_2/Graphene	155 F g^{-1} at 0.5 A g^{-1} 90 F g^{-1} at 1 A g^{-1}	*Dalton Trans.* **2016**, 45, 2637.

Table S4. Comparisons of energy and power density of 1T-MoS_2/$Ti_3C_2T_x$ based flexible ASC with those of asymmetric devices reported recently.

Asymmetric devices	Energy and power density	Refs.
1T-MoS_2@ $Ti_3C_2T_x$ //δ-MnO_2	75 μWh cm^{-2}at 2250 μW cm^{-2} 56.25 μWh cm^{-2} at 27000 μW cm^{-2}	Our work
Co-Al-LDH//$Ti_3C_2T_x$	10.8 μWh cm^{-2} at 250 μW cm^{-2}	*Nano Energy*. **2018**, 50, 479.
Cu $(OH)_2$/CPCC//AC/CC	0.49 μWh cm^{-2} at 600 μW cm^{-2}	*Chem. Eng. J.* **2019**, 371, 348.
NiO@MnO_2//Fe_2O_3	5.6 μWh cm^{-2} at 1680 μW cm^{-2} 9.62 μWh cm^{-2} at 28.9 μW cm^{-2}	*Chem. Eng. J*. **2018**, 347, 101.
CDCC//MnO_2/CDCC	30.1 μWh cm^{-2} at 150 μW cm^{-2} 5.8 μWh cm^{-2} at 7500 μW cm^{-2}	*Electrochim. Acta.* **2018**, 285, 262.
MnO_2//Ppy@MWCNT	12.16 μWh cm^{-2} at 136.8 μW cm^{-2}	*Small.* **2018**, *14*, 1801809.
FCNO/GF//CNR/GF	16.76 μWh cm^{-2} at 69.94 μW cm^{-2}	*Nano Res.* **2018**, 11, 1775–1786.
Ti_3C_2/Fe-15%//MnO_2/CC	42 μWh cm^{-2} at 1600 μW cm^{-2} 20 μWh cm^{-2} at 8200 μW cm^{-2}	*Electrochim. Acta.* ***2019**.308.1*.
RuO_2//$Ti_3C_2T_x$	37 μWh cm^{-2} at 40000 μW cm^{-2}	*Adv. Energy Mater*. **2018**, 8, 1703043.
Bi_2O_3//MnO_2	43.4 μWh cm^{-2} at 12900 μW cm^{-2}	*Adv. Energy Mater.* **2015**, 5, 1401882.
RGO/MnO_2//RGO	35.1 μWh cm^{-2} at 37.5 μW cm^{-2} 11.5 μWh cm^{-2} at 3800 μW cm^{-2}	*Adv. Mater.* **2013**, *25*, 2809.
Poly-PNBTH//VACNT	23.5 μWh cm^{-2} at 14000 μW cm^{-2}	*ACS Appl. Polym. Mater.* **2019**, 1, 1634.
P-TiON//MN	32.4 μWh cm^{-2} at 900 μW cm^{-2} 21.9 μWh cm^{-2} at 4500 μW cm^{-2}	*Adv. Energy Mater*. **2020**, 10, 2001873.
V_2O_5//G-VNQD	73.9 μWh cm^{-2} at 3770 μW cm^{-2}	*Adv. Energy Mater*. **2018**, 8, 1800408.
MnO_2/CNT//PI/CNT	36.4 μWh cm^{-2} at 780 μW cm^{-2} 30.2 μWh cm^{-2} at 15600 μW cm^{-2}	*Carbon*. **2017**, 125, 595-604.